Quantitative evaluation of facet deflection, strain and failure load during simulated cervical spine trauma

Quarrington, R[1,2,3], Costi, J[4], Freeman, B[2,3] and Jones, C[1,2,3]
[1] School of Mechanical Engineering, University of Adelaide; [2] Adelaide Medical School, University of Adelaide; [3] Adelaide Centre for Spinal Research; [4] Biomechanics & Implants Research Group, Flinders University

Word count: 3500 words

ABSTRACT

Traumatic cervical facet dislocation (CFD) is often associated with devastating spinal cord injury. The injury mechanisms leading to CFD are complex and have not been replicated in biomechanical testing; however, anterior shear and flexion loading modes are likely associated with dislocation. Concomitant facet fracture is commonly observed in cases of CFD, yet quantitative measures of facet strain, stiffness and failure load have not been reported. The aim of this study was to determine the mechanical response of the facets when loaded in directions thought to be associated with traumatic CFD. Thirty functional spinal units (FSUs; 6×C2/3, C3/4, C4/5, C5/6 and C6/7) were dissected from thirteen fresh-frozen human cadaver cervical spines (mean age = 70 years [range 48-92], seven male). Uniaxial, low-rate loading was applied to the inferior facets of the inferior vertebra in directions to simulate in-vivo 1) flexion and 2) anterior shear loading. Specimens were subjected to sub-failure loading (10 to 100N) in each direction before being failed in a randomly assigned direction. Facet strain, stiffness, deflection and failure load were measured. Paired and independent t-tests were used for comparison of non-destructive and destructive parameters, respectively ($\alpha=0.05$). Facet stiffness and failure load were significantly greater in flexion, and facet deflection and surface strain were higher in the anterior shear loading direction. Failure occurred through the facet tip when subjected to anterior shear loading, while failure through the pedicles was most common for simulated flexion loading. Subsequent linear mixed effects models will be used to account for vertebral level, donor demographics, and bone quality. It is anticipated that this information will be used to validate and inform computational models of cervical trauma and will assist with the development of preventative measures.

INTRODUCTION

Traumatic cervical facet dislocation (CFD) is often associated with devastating spinal cord injury (SCI), resulting in tetraplegia in up to 87% of cases (Hadley, 1992; Payer, 2005). In Australia, tetraplegia cases reported in a 2008 cohort amounted to annual care costs of AUD$14.6 million (Access Economics Pty Limited, 2009). CFD occurs most frequently, and is most often survivable, in the sub-axial region (C3-T1). It can occur uni- or bilaterally, with bilateral facet dislocation (BFD) more frequently resulting in complete neurological injury (Allen, 1982; Quarrington, unpublished).

CFD is commonly a result of traffic and sporting accidents, and falls (Allen, 1982; Quarrington, unpublished), during which the loading mechanisms are complex and highly variable; the mechanisms of facet dislocation have not been replicated in biomechanical testing (Foster, 2012). BFD is thought to result from combined flexion-distraction loading due to axial compressive forces applied to the head with large anterior eccentricity (Allen, 1982; Cusick, 2002; White, 1990). This mechanism was proposed in a seminal radiographic study (Allen, 1982) and has only been validated in one series of experiments (Ivancic, 2007, 2008; Panjabi, 2007) in which the incremental inertial loading method used may not be representative of a majority of real-life cervical trauma. Several other studies have produced BFD experimentally using low-rate loading, or through soft-tissue disruption in combination with manual manipulation (Bauze, 1978; Beatson, 1963; Kim, 2004; Roaf, 1960; Sim, 2000). Facet dislocation injuries have been observed following dynamic compression loading (Maiman, 1983; Nightingale, 1991; Tsai, 1997) and head impact testing (Hodgson, 1980; Ivancic, 2012; Nightingale, 1996; Pintar, 1995; Saari, 2011) of cadaver cervical spines; however, the injury mechanisms of BFD were not the focus of these studies.

Panjabi *et al*. (2007) identified flexion-distraction and anterior shear, followed by axial compression, as the dominant sagittal motions observed during the experimental production of BFD. In that study, the kinematic analysis assumed that the vertebrae (including posterior elements) were perfectly rigid bodies during the traumatic motion. Other studies which measured kinematics of cervical functional spinal units (FSUs) during spinal motion have applied the same assumption (Cook, 2010; Ivancic, 2007, 2008). Sagittal bending of the facets relative to the vertebral body in excess of 14 degrees during replicated physiological flexion motion has been observed in the lumbar region (Green, 1994), but no equivalent data is available for the cervical vertebrae. Additionally, concomitant facet fracture is associated with CFD in up to 79% of cases (Piccirilli, 2013), and one could expect substantial bending of the facets to occur prior to mechanical failure. The magnitude of facet deflection in the subaxial cervical spine during simulated traumatic motion has not been reported.

To our knowledge, no studies have quantified the response of the cervical facets to traumatic mechanical loading. Investigations of the load-bearing capacity (Hakim, 1976; King, 1975; Pollintine, 2004), failure mechanisms (Cyron, 1976), fatigue strength (Cyron, 1978) and strain response (Schulitz, 1980; Shah, 1978; Suezawa, 1980) of the *lumbar* facets and neural arch have been performed, but a similar analysis has not been reported for the subaxial cervical spine, or during simulated facet dislocation. Other studies have directly measured facet joint contact pressure (Jaumard, 2011a; Jaumard, 2011b) and surface strain (Wang, 2012), and indirectly measured facet joint force (Chang, 2007) in the cervical spine; however, these studies did not replicate traumatic cervical motion. Quantitative measures of the mechanical response of the cervical facets to simulated traumatic loading may be important parameters for validation of computational models of trauma and to inform design of advanced anthropometric test device (ATD) necks and associated injury criteria.

The aim of this study was to quantify the deflection, apparent stiffness, surface strain and failure load of the inferior facets under uni-axial loads (applied to their articular surface to simulate contact with the articulating superior facet) which simulated the loading mechanisms thought to cause BFD – anterior shear and flexion (Panjabi, 2007).

METHODS

Specimen preparation

Thirty functional spinal units (FSUs; 6×C2/3, C3/4, C4/5, C5/6 and C6/7) were dissected from thirteen fresh-frozen human cadaver cervical spines. Mean age of the donors was 70 years (range 48-92); seven were male and six were female. Radiographs and computed tomography (CT) scans were obtained and each specimen was screened for excessive degeneration, injury and disease by a spinal surgeon. Average volumetric bone mineral density for each specimen was quantified from CT using a calibration phantom (Mindways Software Inc., USA) and image analysis software (FIJI). Musculature was removed and the vertebral disc and bilateral facet joint capsules were preserved (Figure 1a). Articular cartilage was removed from the inferior facets of the inferior vertebrae.

The vertebral bodies of each FSU were embedded in polymethylmethacrylate (PMMA) using a custom adjustable mold (Figure 1b). To assist with fixation, a long wood-screw was inserted through the vertebral bodies and disc, and steel wire was wrapped around the vertebral bodies through the transverse foramen; excess wire and the screw-tip protruded from the superior endplate of the superior vertebra into a rectangular embedding cavity approximately 50 mm in length. The FSU was positioned in the mold with the spinous processes pointing vertically, perpendicular to the base, such that the posterior surfaces of the vertebral bodies aligned with the top surface of the mold. The lateral anatomy was pressed into plasticine to hold the specimen in the desired orientation, and to prevent the facets being embedded. The mold was then filled with PMMA. Once set, a thin steel bar was positioned within the spinal canal along the posterior surfaces of the vertebral bodies and the PMMA block, and was fixed using a thin layer of PMMA (Figure 1b and c). The embedded specimen was then removed from the mold for instrumenting.

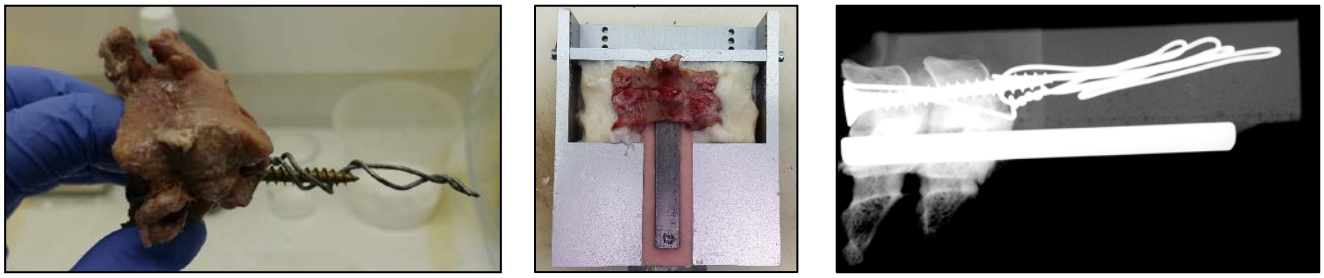

a **b** **c**

Figure 1: Specimen preparation: a) cervical functional spinal unit dissected of soft-tissue, with wood-screw and steel wire attached to vertebral bodies; b) custom potting cup for embedding the specimen in PMMA, and; c) lateral radiograph of the embedded specimen.

Mechanical loading

The specimen-PMMA assembly was rigidly mounted to the base of a biaxial materials testing machine (8874, Instron, UK) via a custom support apparatus attached to a rotary table (Figure 2). Using the rotary table, the inferior articular facet surfaces of the inferior vertebrae were positioned relative to the actuator to simulate in-vivo 1) flexion and 2) anterior shear loading

(Figure 2). The simulated flexion loading direction was applied perpendicular to the facet surface, while anterior-shear loading was applied parallel to the inferior vertebral endplate; the posterior elements of the superior vertebra provided a physiological boundary condition to the loaded inferior facets. Three cycles of uniaxial sub-failure loading to 100 N (10 N pre-load) were applied bilaterally to the geometric centre of each articular facet surface at 1 mm/s using 6 mm diameter hemispherical loading pins, in each loading direction. The span of the loading pins was equal to the distance between the facet centres and symmetric about the line of action of the actuator. The non-destructive load limit was determined from pilot testing. Following completion of the sub-failure testing, each specimen was loaded to failure in a randomly assigned direction at 10 mm/s. The non-destructive and destructive loading rates chosen were the maximum possible to obtain adequate motion-capture data and maintain control of the test machine.

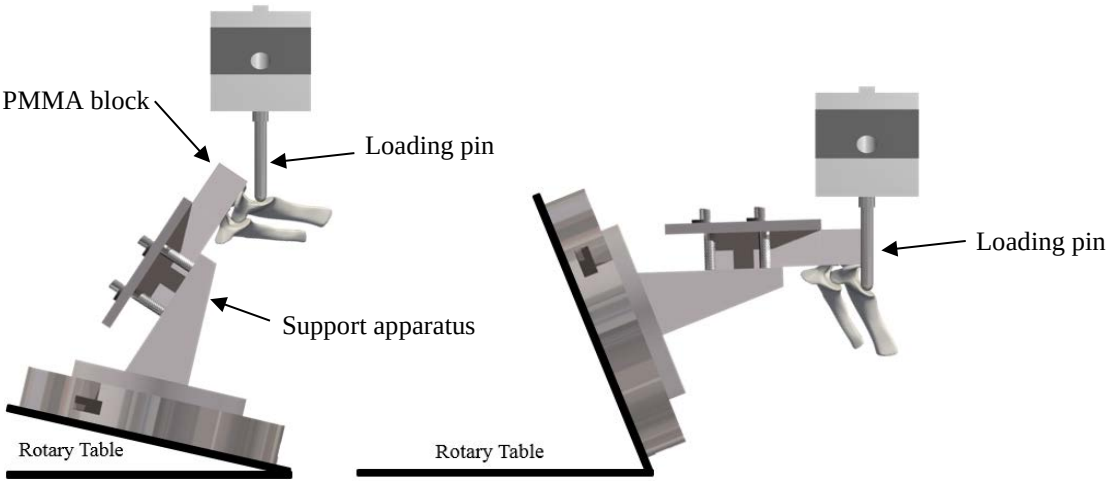

Figure 2: Side-view schematic of the mechanical testing setup for simulated flexion (left) and anterior shear (right) loading.

Instrumentation and data collection

The inferior vertebra of each specimen was instrumented to measure the mechanical response of the bilateral inferior facets to loading. Tri-axial rosette strain gauges (FRA-1-23-1L, TML, Japan) and custom light-weight motion capture marker-carriers (Optotrak Certus, Northern Digital Inc., Canada) were fixed to the bilateral inferior facet bases and tips, respectively (Figure 3). Rosette gauges were positioned such that the +45° strain gauge coincided with the mid-sagittal plane of each facet. A third marker-carrier was attached to the inferior vertebral body via a K-wire (Figure 3).

Figure 3: Specimens instrumented with tri-axial rosette strain gauges (left) and custom Optotrak marker-carriers (right).

The following anatomical landmarks on the inferior vertebra were digitised using a 1mm diameter spherical probe tip: the antero-lateral, postero-lateral, and postero-medial 'corners' of the left and right inferior articular facet surfaces; and, the four corners of the inferior endplate (Figure 4). Three-dimensional marker coordinates were collected at 300 Hz.

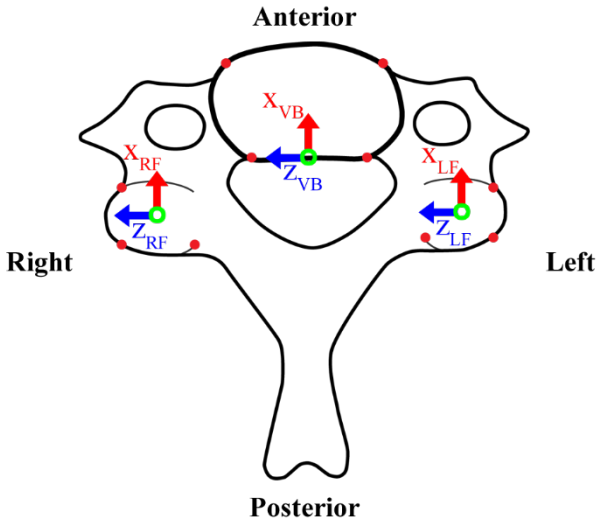

Figure 4: A schematic of the inferior view of a cervical vertebra, where the red dots indicate the anatomical landmarks that were digitised. The local coordinate systems are illustrated, with x-axes in red, z-axes in blue, and the origins in green.

Loads and actuator position were measured by a biaxial load cell (Dynacell ±25 kN, Instron, UK) and internal linear variable differential transformer (LVDT), respectively. A six-axis load cell (MC3A-6-1000, AMTI, USA) was connected in series to measure off-axis loads and moments. Voltage output from the strain gauges, Instron (load cell, LVDT and trigger signal), and six-axis load cell were collected at 600 Hz using a data acquisition system (PXIe-1073 + BNC-2120 & PXIe-4331 (x2), National Instruments, USA). This data was synchronised with the motion-capture data in post-processing using the recorded trigger signal. Failure tests were filmed at 100Hz using a high-speed camera (i-Speed TR, Olympus, Japan).

Data processing

Data were processed using custom MATLAB code (R2015a, Mathworks, USA). Strain gauge, motion capture, LVDT, and load cell data were filtered using a second-order, two-way Butterworth low-pass filter at cut-off frequencies of 40, 30, 80, and 100 Hz, respectively. LVDT and load cell voltages were converted to position (mm) and load (N) values using the calibration coefficients provided by the manufacturers. Cross-talk between axes in the six-axis load cell was corrected using the sensitivity matrix specified by AMTI.

The aforementioned 25kN biaxial load cell was used to control the 100N axial load-limit for each test; however, a substantial anterior-shear load occurred during the simulated anterior-shear tests, due to the inclined angle of the facets in this specimen orientation. Therefore, to ensure the outcome measures for each specimen were determined at an equivalent load, the resultant sagittal load ($\sqrt{[\text{axial load}^2 + \text{anterior-shear load}^2]}$) was calculated for each test, and the outcome measures corresponding to a resultant of 60 N (the highest load reached by all specimens) were determined. Axial load-displacement plots were generated for the sub-failure tests, and apparent axial facet stiffness (N/mm) was determined from the slope of the linear region. Principal strains were calculated from the output of each rosette gauge.

Local anatomical coordinate systems, consistent with ISB recommendations for spinal joints (Wu, 2002), were defined for the vertebral body and facets using the anatomical landmark coordinates illustrated in Figure 4. Angular deflection of the facets relative to the vertebral body (in degrees) was calculated by solving for Euler angles using a *z*-*y*-*x* sequence (Robertson, 2004). For the destructive tests, the instant of initial failure (of either one or both facets, defined as a distinct drop in load and confirmed using high-speed camera footage) was identified and the axial load, facet deflection and principal strains were determined at this point. The failure mode of each specimen was determined from viewing the high-speed camera footage and by visual inspection of the specimen.

Statistics

Data from the last cycle of each test were used for statistical analysis. Where anatomical asymmetry led to loading asymmetry, the larger of the two strain and deflection values were used. Paired t-tests (α=0.05) were used to compare facet deflection, maximum principal strain and apparent axial stiffness values measured at 60 N between loading directions, for each specimen. Independent t-tests (α=0.05) were used to compare outcome parameters at initial failure between those specimens failed during simulated flexion, and those failed in the anterior-shear loading direction. For this analysis, FSUs from different vertebral levels were grouped together.

RESULTS

One C3/4 specimen was omitted from all analyses due to technical complications during testing. Failure data was not available for a further six specimens due to: inadequate fixation of the specimen in the embedding material (N=2; C3/4 and C5/6); poor bone quality resulting in loading pins puncturing the facets (N=3; C2/3, C4/5 and C5/6); and, slipping of the rotary table (N=1; C4/5). Donor and specimen details, and failure outcomes are provided in Table 1.

Table 1: Donor and specimen details, and failure test outcome measures. vBMD = volumetric K2HPO4 equivalent bone mineral density (mg/cm3). 'NA' indicates that failure data was not available. Test 1 omitted due to technical difficulties

Test #	Specimen ID	Spinal Level	Sex	Age	Average vBMD	Failure Direction	Failure Load (N)	Failure Location
2	H023	C5C6	M	92	-27.3	NA	NA	NA
3	H001	C2C3	M	48	192.2	Anterior Shear	225.8	Facet Tips
4	H001	C4C5	M	48	293.5	NA	NA	NA
5	H001	C6C7	M	48	212.9	Anterior Shear	470.6	Facet Tips
6	H027	C3C4	F	64	177.7	Anterior Shear	337.9	Facet Tips
7	H012	C2C3	F	67	434.7	Flexion	804.1	Pedicles
8	H027	C5C6	F	64	142.2	Anterior Shear	337.0	Facet Tips
9	H012	C4C5	F	67	140.2	Anterior Shear	326.7	Facet Tips
10	H012	C6C7	F	67	118.5	Anterior Shear	292.4	Facet Tips
11	H017	C4C5	F	86	27.6	Anterior Shear	121.2	Facet Tips
12	H017	C2C3	F	86	34.3	NA	NA	NA
13	H006	C3C4	M	57	238.5	NA	NA	NA
14	H032	C6C7	M	65	161.0	Flexion	590.1	Facet Tips
15	H032	C2C3	M	65	161.0	Anterior Shear	316.3	Facet Tips
16	H006	C5C6	M	57	207.4	NA	NA	NA
17	H032	C4C5	M	65	171.9	NA	NA	NA
18	H045	C5C6	F	74	121.6	Anterior Shear	417.1	Facet Tips
19	H045	C3C4	F	74	136.6	Anterior Shear	404.7	Facet Tips
20	H039	C6C7	F	86	92.9	Flexion	877.1	Facet Tips
21	H039	C4C5	F	86	156.3	Flexion	1021.4	Facet Bases
22	H039	C2C3	F	86	194.2	Anterior Shear	366.1	Facet Tips
23	H018	C4C5	M	84	207.6	Flexion	1054.2	Pedicles
24	H018	C6C7	M	84	179.1	Anterior Shear	558.6	Facet Tips
25	H018	C2C3	M	84	209.2	Flexion	852.5	Pedicles
26	H026	C5C6	M	74	145.0	Anterior Shear	379.0	Facet Tips
27	H026	C3C4	M	74	140.4	Flexion	765.7	Pedicles
28	H021	C3C4	F	61	216.2	Flexion	639.0	Pedicles
29	H021	C5C6	F	61	179.6	Flexion	1203.2	Facet Bases
30	H044	C6C7	M	62	118.7	Flexion	721.4	Pedicles

Specimens demonstrated significantly greater apparent facet stiffness when loaded in the flexion direction compared to the anterior shear loading direction (Figure 5). Stiffness values ranged from 99.4 to 543.8 (mean = 258.8±103.2) N/mm for flexion loading, and from 29.1 to 210.0 (mean = 101.8±51.7) N/mm for anterior shear. These stiffness measurements corresponded with significantly larger maximum principal strains and sagittal facet deflections for the anterior shear loading direction (Figure 5). Facet deflections were only appreciable in the sagittal plane.

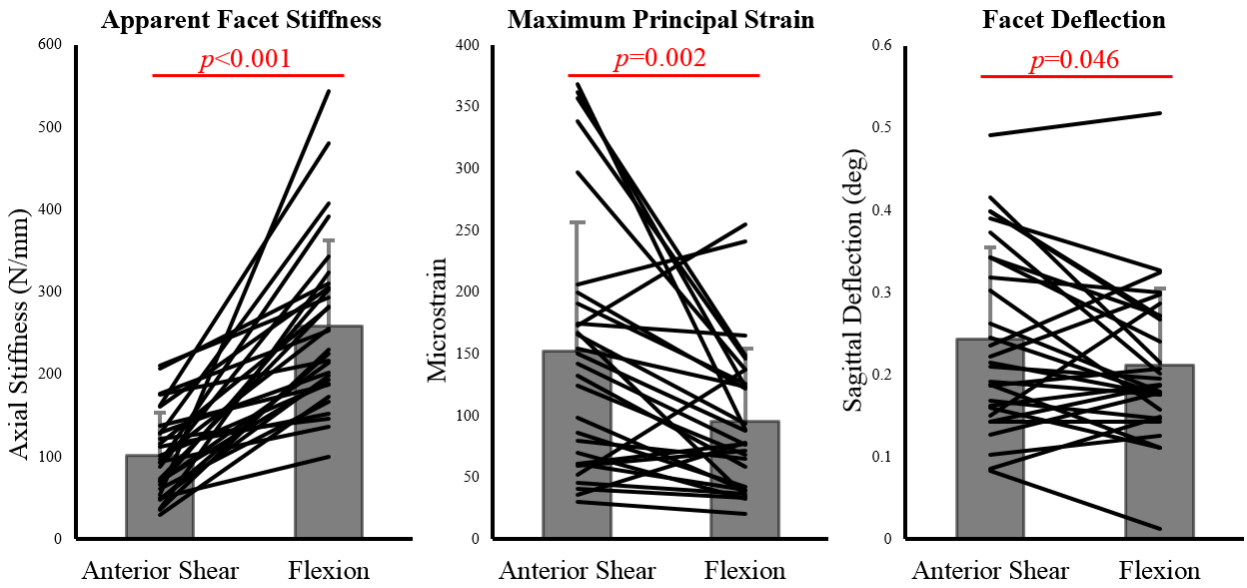

Figure 5: Plots of apparent axial facet stiffness (left), maximum principal strain (centre), and sagittal facet deflection (right) measured at 60N from the non-destructive tests. Each black line represents the paired anterior shear and flexion results for a single specimen, and the semi-transparent bars illustrate the mean (+1 SD) of all specimens for each loading direction.

Axial failure load and sagittal facet deflection at failure were significantly higher for those specimens that were failed in the simulated flexion loading direction than for those failed in anterior shear (Figure 6). The highest failure load was 1.26 kN, and sagittal facet deflections ranged from 1.34 to 5.39 (mean = 2.64±1.11) degrees for anterior shear and from 2.55 to 12.95 (mean = 6.08±3.17) degrees for flexion. There was no statistical difference between the maximum principal strains observed at failure for the two loading directions.

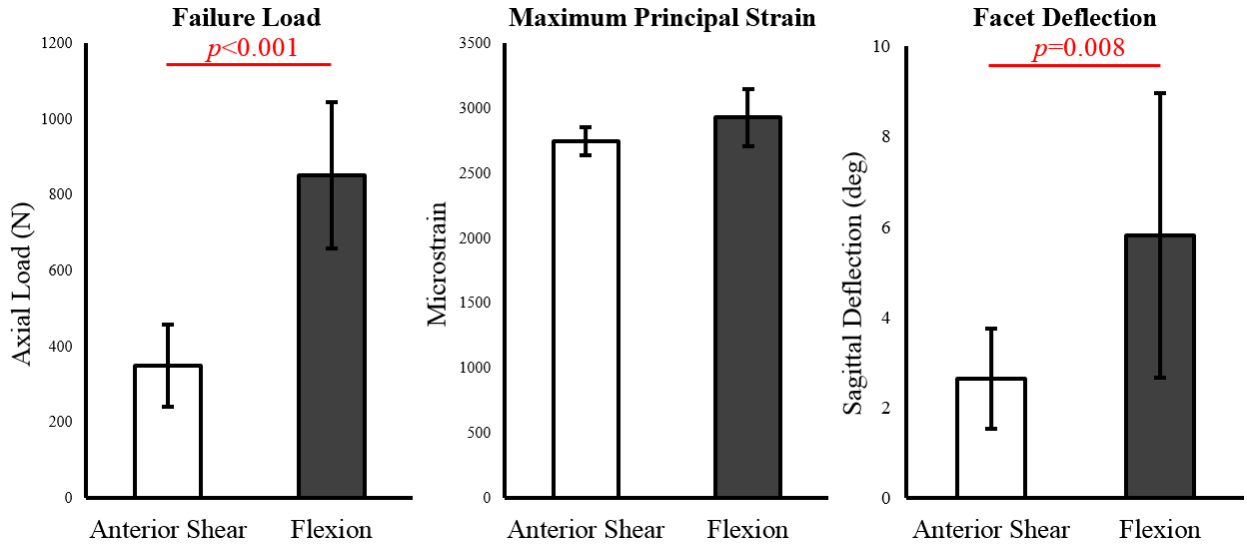

Figure 6: Mean (±1 SD) axial load (left), maximum principal strain (centre), and sagittal facet deflection (right) measured at initial failure for simulated anterior shear and flexion loading.

Two distinct fracture locations were identified (Figure 7). All specimens that were loaded destructively in the anterior shear direction failed through the inferior facet tips (13/13 specimens; Table 1). Of the ten specimens tested to failure under simulated flexion loading, six fractured through the pedicles, and two each fractured through the facet bases and facet tips (Table 1).

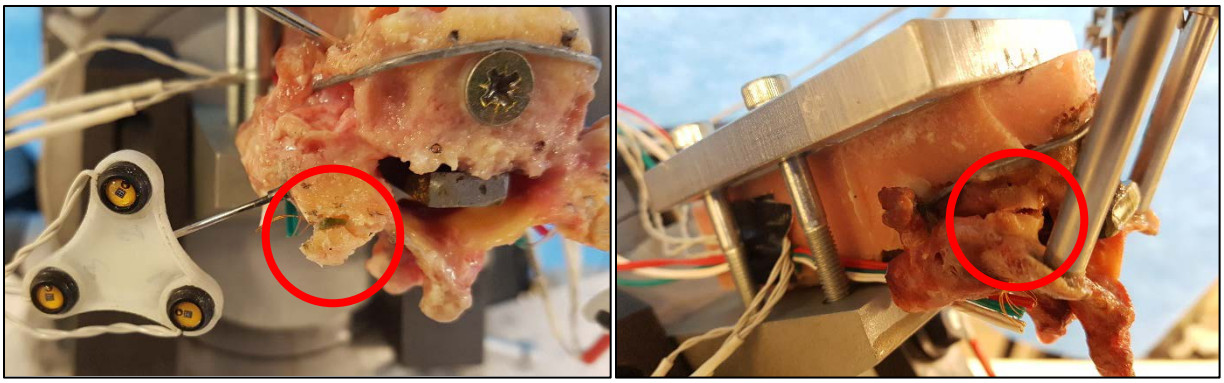

Figure 7: Photographs of the typical failure locations (indicated by the red circles) for specimens loaded in the replicated anterior shear (left) and flexion (right) loading directions.

DISCUSSION

Despite the potentially devastating consequences of CFD, very little published data exists regarding the biomechanics underlying this injury mechanism. In particular, the mechanical response of the subaxial facets, which are often fractured during CFD (Allen, 1982; Piccirilli, 2013), has not previously been investigated. Quantitative measures of this mechanical response are required to validate computational models of cervical trauma and may assist with design of improved ATDs and neck injury criteria.

In the present study, bilateral uniaxial loading was applied to the inferior facets of subaxial cervical vertebrae in directions that replicate traumatic anterior shear and flexion; these motions are commonly associated with CFD (Allen, 1982; Cusick, 2002; White, 1990). Rosette strain gauges were used to determine principal strains at the bilateral facet bases. It was hypothesized that facet bending would occur about this region, and that this strain measure may be dependent on loading direction. Maximum principal strains were significantly larger at 60 N of applied anterior shear load than for the equivalent flexion tests (Figure 5). This is in agreement with the larger deflection and reduced stiffness values observed for the non-destructive anterior shear tests. Interestingly, no difference in maximum strain at failure was observed between loading directions (Figure 6). This could be attributed to the lower failure load observed for those specimens failed in the anterior shear loading direction.

There is little published data regarding cervical facet surface strains with which to compare our results. Wang *et al*. (2012) measured average C3 and C4 inferior facet strains of 42.3 and 37.7 microstrain (με), respectively, at 20 degrees of flexion; they did not apply anterior shear. These values are less than 50% of the average maximum principal strains obtained during non-destructive flexion testing in our study (Figure 5). This may suggest that our sub-failure analysis load of 60 N is greater than that experienced by the facets *in-vivo* during physiological flexion motion of the

cervical spine. As such, *in-vivo* facet deflections may be as low as ~0.1 degrees during 20 degrees of cervical flexion. This will be investigated directly in our next study. Maximum principal strains at failure ranged from 833.7 to 6889.3 (mean = 2744.7±1696.9) με for anterior shear, and from 938.3 to 5692.0 (mean = 2844.6±1707.4) με for flexion. We are currently developing a computational model of cervical trauma and will use this experimental data to validate the facet strains estimated by the model.

Angular deflections of the cervical facets (relative to the vertebral body) in excess of 12 degrees were measured at failure. This is comparable to observations of over 14 degrees of sagittal bending of the *lumbar* facets during replicated physiological flexion motion (Green, 1994). Specimens that were failed under flexion loading demonstrated significantly larger sagittal deflections at initial failure than those failed in anterior shear (Figure 6). These large deflections prior to facet fracture suggest that the anterior and posterior elements of the vertebrae are not perfectly rigid during cervical trauma, and should not be assumed to act as such during kinematic analysis of motion segment injury involving the posterior anatomy.

The mechanism of failure was distinctly different for the two loading modes, and this difference was associated with significantly different axial failure loads (Figure 6). Bending of the facets during anterior shear loading caused the point of load application to translate inferiorly towards the facet tip. As this translation occurred, the volume of bone beneath the loading pin decreased until fracture occurred through the facet tip. This fracture location is consistent with that described in radiographic reports of distractive-flexion injury mechanisms (Allen, 1982). In contrast, for most specimens that were failed in the simulated flexion orientation, the point of contact of the loading pin remained constant, until failure occurred through the pedicles or the facet base (Table 1). A finite element model of cervical trauma identified high stresses in these regions prior to failure during flexion (DeWit, 2012). Substantial translation of the loading pin was observed in the two flexion specimens that fractured through the facet tip.

The axial failure loads for pedicle fractures observed in our study were considerably lower than those recorded for the lumbar spine (Cyron, 1976), probably due to the smaller size of the cervical vertebrae. No similar data exists for the cervical posterior elements, although failure load of the C2 odontoid process was similar (Teo, 2001). We propose that future ATD design may be improved by including load cells in the posterior cervical spine, and this data may be useful for developing associated injury criteria.

The testing protocol implemented in this study was unable to replicate facet loading experienced during traumatic axial-rotation, and had some limitations in regards to boundary and loading conditions. Bilateral, sagittal-plane, loading was applied to simulate two of the loading modes thought to cause BFD; however, facet fracture is more commonly associated with unilateral dislocation (UFD) (Argenson, 1988). Combined axial rotation and flexion injury mechanisms are thought to be the primary causes of UFD (Argenson, 1988; Bauze, 1978; White, 1990), resulting in oblique, unifacet loading. It was not possible to simulate axial rotation in the described manner as the required line of action of force would pass through the vertebral body; however, we plan to investigate this using an FSU model.

The superior adjacent vertebra provided a physiological boundary condition for the loaded posterior elements. Pilot testing demonstrated that facets were stiffer, and deflections and strains were larger, when the adjacent facets were present compared to after they were resected. However, we were unable to apply a boundary condition to the inferior vertebral endplate that replicated the inferior vertebral body at the level of injury. We believe that such a boundary condition may influence the failure mechanisms observed as interference of the anterior elements may restrict large flexion motions (Allen, 1982). This boundary condition will be satisfied in our experimental FSU model of CFD.

To permit the same loading method for both loading directions, hemispherical loading pins were used to apply point loads to the facets; however, point loading is likely not representative of *in-vivo* facet loading conditions, and might induce higher stresses at the point of application. These point stresses could have resulted in the 'punctured' facet failure mode that occurred for three specimens, although the clinically relevant fractures observed for most specimens suggests that this was not a significant limitation and that poor bone quality may have been the primary cause. Linear mixed-effects models are currently being developed to adjust for specimen variation in bone quality (vBMD), donor demographics, and spinal level, and identify statistically significant associations between loading direction and the mechanical response of the facets.

CONCLUSIONS

The present study provides information about the mechanical response of the subaxial cervical inferior facets when loaded in the directions that simulate the injury mechanisms of cervical facet dislocation. The cervical facets tended to be stiffer, and have a higher failure load, when loaded in flexion, and this corresponded with larger sagittal angular deflections and higher facet surface strain in the anterior shear loading direction. Facet tip fracture occurred in all specimens that were loaded to failure in anterior shear, while fracture through the pedicles was most common for the destructive flexion tests. We anticipate that the information gained in this study will be used to validate and inform computational models of cervical trauma, and may assist with the development of improved neck injury criteria for ATDs.

ACKNOWLEDGEMENTS

Funding was provided by AOSpine Australia New Zealand (AOSAUNZ2015-03), the Royal Adelaide Hospital Research Fund, and the Australian Government's Research Training Program. C Jones is supported by a National Health and Medical Research Council (Australia) Early Career Fellowship.

REFERENCES

ACCESS ECONOMICS PTY LIMITED (2009). The Economic Cost of Spinal Cord Injury and Traumatic Brain Injury in Australia. The Victorian Neurotrauma Initiative.

ALLEN, B.L., JR., FERGUSON, R.L., LEHMANN, T.R., O'BRIEN, R.P. (1982). A Mechanistic Classification of Closed, Indirect Fractures and Dislocations of the Lower Cervical Spine. Spine 7, 1-27.

ARGENSON, C., LOVET, J., SANOUILLER, J.L., DE PERETTI, F. (1988). Traumatic Rotatory Displacement of the Lower Cervical Spine. Spine 13, 767-773.

BAUZE, R.J., ARDRAN, G.M. (1978). Experimental Production of Forward Dislocation in the Human Cervical Spine. The Journal of bone and joint surgery. British volume 60-B, 239-245.

BEATSON, T.R. (1963). Fractures and Dislocations of the Cervical Spine. Journal of Bone and Joint Surgery 45-B, 21-35.

CHANG, U.K., KIM, D.H., LEE, M.C., WILLENBERG, R., KIM, S.H., LIM, J. (2007). Changes in Adjacent-Level Disc Pressure and Facet Joint Force after Cervical Arthroplasty Compared with Cervical Discectomy and Fusion. Journal of neurosurgery. Spine 7, 33-39.

COOK, D.J., CHENG, B.C. (2010). Development of a Model Based Method for Investigating Facet Articulation. Journal of biomechanical engineering 132, 064504.

CUSICK, J.F., YOGANANDAN, N. (2002). Biomechanics of the Cervical Spine 4: Major Injuries. Clinical biomechanics 17, 1-20.

CYRON, B.M., HUTTON, W.C., TROUP, J.D. (1976). Spondylolytic Fractures. The Journal of bone and joint surgery. British volume 58-B, 462-466.

CYRON, B.M., HUTTON, W.C. (1978). The Fatigue Strength of the Lumbar Neural Arch in Spondylolysis. The Journal of bone and joint surgery. British volume 60-B, 234-238.

DEWIT, J.A., CRONIN, D.S. (2012). Cervical Spine Segment Finite Element Model for Traumatic Injury Prediction. J Mech Behav Biomed Mater 10, 138-150.

FOSTER, B.J., KERRIGAN, J.R., NIGHTINGALE, R.W., FUNK, J.R., CORMIER, J.M., BOSE, D., SOCHOR, M.R., RIDELLA, S.A., ASH, J.H., CRANDALL, J. (Year) Analysis of Cervical Spine Injuries and Mechanisms for Ciren Rollover Crashes. In 2012 International IRCOBI Conference on the Biomechanics of Injury. Dublin, Ireland.

GREEN, T.P., ALLVEY, J.C., ADAMS, M.A. (1994). Spondylolysis. Bending of the Inferior Articular Processes of Lumbar Vertebrae During Simulated Spinal Movements. Spine 19, 2683-2691.

HADLEY, M.N., FITZPATRICK, B.C., SONNTAG, V.K., BROWNER, C.M. (1992). Facet Fracture-Dislocation Injuries of the Cervical Spine. Neurosurgery 30, 661-666.

HAKIM, N.S., KING, A.I. (Year) Static and Dynamic Articular Facet Loads. In 20th Stapp Car Crash Conference. Dearborn, MI.

HODGSON, V., THOMAS, L. (1980). Mechanisms of Cervical Spine Injury During Impact to the Protected Head. SAE Technical Paper 801300.

IVANCIC, P.C., PEARSON, A.M., TOMINAGA, Y., SIMPSON, A.K., YUE, J.J., PANJABI, M.M. (2007). Mechanism of Cervical Spinal Cord Injury During Bilateral Facet Dislocation. Spine 32, 2467-2473.

IVANCIC, P.C., PEARSON, A.M., TOMINAGA, Y., SIMPSON, A.K., YUE, J.J., PANJABI, M.M. (2008). Biomechanics of Cervical Facet Dislocation. Traffic injury prevention 9, 606-611.

IVANCIC, P.C. (2012). Biomechanics of Sports-Induced Axial-Compression Injuries of the Neck. Journal of athletic training 47, 489-497.

JAUMARD, N.V., BAUMAN, J.A., WEISSHAAR, C.L., GUARINO, B.B., WELCH, W.C., WINKELSTEIN, B.A. (2011a). Contact Pressure in the Facet Joint During Sagittal Bending of the Cadaveric Cervical Spine. Journal of biomechanical engineering 133, 071004.

JAUMARD, N.V., BAUMAN, J.A., WELCH, W.C., WINKELSTEIN, B.A. (2011b). Pressure Measurement in the Cervical Spinal Facet Joint: Considerations for Maintaining Joint Anatomy and an Intact Capsule. Spine 36, 1197-1203.

KIM, S.M., LIM, T.J., PATERNO, J., PARK, J., KIM, D.H. (2004). A Biomechanical Comparison of Three Surgical Approaches in Bilateral Subaxial Cervical Facet Dislocation. Journal of neurosurgery. Spine 1, 108-115.

KING, A.I., PRASAD, P., EWING, C.L. (1975). Mechanism of Spinal Injury Due to Caudocephalad Accleration. The Orthopedic clinics of North America 6, 19-31.

MAIMAN, D.J., SANCES, A., JR., MYKLEBUST, J.B., LARSON, S.J., HOUTERMAN, C., CHILBERT, M., EL-GHATIT, A.Z. (1983). Compression Injuries of the Cervical Spine: A Biomechanical Analysis. Neurosurgery 13, 254-260.

NIGHTINGALE, R.W., DOHERTY, B.J., MYERS, B.S., MCELHANEY, J.H., RICHARDSON, W.J. (1991). The Influence of End Condition on Human Cervical Spine Injury Mechanisms, SAE Technical Paper 912915.

NIGHTINGALE, R.W., MCELHANEY, J.H., RICHARDSON, W.J., MYERS, B.S. (1996). Dynamic Responses of the Head and Cervical Spine to Axial Impact Loading. Journal of biomechanics 29, 307-318.

PANJABI, M.M., SIMPSON, A.K., IVANCIC, P.C., PEARSON, A.M., TOMINAGA, Y., YUE, J.J. (2007). Cervical Facet Joint Kinematics During Bilateral Facet Dislocation. Eur. Spine J. 16, 1680-1688.

PAYER, M., SCHMIDT, M.H. (2005). Management of Traumatic Bilateral Locked Facets of the Subaxial Cervical Spine. Contemp. Neurosurg. 27, 1-3.

PICCIRILLI, M., LIBERATI, C., SANTORO, G., SANTORO, A. (2013). Cervical Post-Traumatic Unilateral Locked Facets: Clinical, Radiological and Surgical Remarks on a Series of 33 Patients. J. Spinal Disord. Tech.

PINTAR, F., YOGANANDAN, N., VOO, L., CUSICK, J.F., MAIMAN, D.J., SANCES, A. (Year) Dynamic Characteristics of the Human Cervical Spine. In 39th Stapp Car Chrash Conference. San Diego, CA.

POLLINTINE, P., PRZYBYLA, A.S., DOLAN, P., ADAMS, M.A. (2004). Neural Arch Load-Bearing in Old and Degenerated Spines. Journal of biomechanics 37, 197-204.

QUARRINGTON, R.D., JONES, C.F., TCHERVENIAKOV, P., CLARK, J.M., SANDLER, S.J., LEE, Y.C., TORABIARDAKANI, S., COSTI, J.J., FREEMAN, B.J. (unpublished). Traumatic Subaxial Cervical Facet Subluxation and Dislocation: Epidemiology, Radiographic Analyses and Risk Factors for Spinal Cord Injury, Manuscript submitted for publication.

ROAF, R. (1960). A Study of the Mechanics of Spinal Injuries. Journal of Bone and Joint Surgery 42B, 810-823.

ROBERTSON, D.G.E. (2004). Research Methods in Biomechanics. Human Kinetics, Champaign, IL.

SAARI, A., ITSHAYEK, E., CRIPTON, P.A. (2011). Cervical Spinal Cord Deformation During Simulated Head-First Impact Injuries. Journal of biomechanics 44, 2565-2571.

SCHULITZ, K.P., NIETHARD, F.U. (1980). Strain on the Interarticular Stress Distribution. Measurements Regarding the Development of Spondylolysis. Arch. Orthop. Trauma Surg. 96, 197-202.

SHAH, J.S., HAMPSON, W.G., JAYSON, M.I. (1978). The Distribution of Surface Strain in the Cadaveric Lumbar Spine. The Journal of bone and joint surgery. British volume 60-B, 246-251.

SIM, E., VACCARO, A.R., BERZLANOVICH, A., PIENAAR, S. (2000). The Effects of Staged Static Cervical Flexion-Distraction Deformities on the Patency of the Vertebral Arterial Vasculature. Spine 25, 2180-2186.

SUEZAWA, Y., JACOB, H.A., BERNOSKI, F.P. (1980). The Mechanical Response of the Neural Arch of the Lumbosacral Vertebra and Its Clinical Significance. Int. Orthop. 4, 205-209.

TEO, E.C., PAUL, J.P., EVANS, J.H., NG, H.W. (2001). Experimental Investigation of Failure Load and Fracture Patterns of C2 (Axis). Journal of biomechanics 34, 1005-1010.

TSAI, K.H., CHANG, G.L., LIN, R.M. (1997). Differences in Mechanical Response between Fractured and Non-Fractured Spines under High-Speed Impact. Clinical biomechanics 12, 445-451.

WANG, C.S., CHANG, J.H., CHANG, T.S., CHEN, H.Y., CHENG, C.W. (2012). Loading Effects of Anterior Cervical Spine Fusion on Adjacent Segments. Kaohsiung J. Med. Sci. 28, 586-594.

WHITE, A.A., PANJABI, M.M. (1990). Clinical Biomechanics of the Spine. Lippincott.

WU, G., SIEGLER, S., ALLARD, P., KIRTLEY, C., LEARDINI, A., ROSENBAUM, D., WHITTLE, M., D'LIMA, D.D., CRISTOFOLINI, L., WITTE, H., SCHMID, O., STOKES, I. (2002). Isb Recommendation on Definitions of Joint Coordinate System of Various Joints for the Reporting of Human Joint Motion--Part I: Ankle, Hip, and Spine. International Society of Biomechanics. Journal of biomechanics 35, 543-548.